Structure of liquid tricalcium aluminate

James W. E. Drewitt,[1,*] Adrian C. Barnes,[2] Sandro Jahn,[3] Simon C. Kohn,[1] Michael J. Walter,[1] Alexey N. Novikov,[4,5] Daniel R. Neuville,[4] Henry E. Fischer,[6] and Louis Hennet[5]

[1]*School of Earth Sciences, University of Bristol, Wills Memorial Building, Queens Road, Bristol, BS8 1RJ, United Kingdom*

[2]*H H Wills Physics Laboratory, University of Bristol, Bristol, BS8 1TL, United Kingdom*

[3]*Institute of Geology and Mineralogy, University of Cologne, Zuelpicher Str. 49b, 50674 Cologne, Germany*

[4]*Institut de Physique du Globe de Paris, CNRS-IPGP, Géomatériaux, Sorbonne Paris Cité, 1 rue Jussieu, 75005 Paris, France*

[5]*Conditions Extrêmes et Matériaux : Haute Température et Irradiation, CEMHTI-CNRS, Université d'Orléans, 1d avenue de la Recherche Scientifique, 45071 Orléans cedex 2, France*

[6]*Institut Laue-Langevin, 71 avenue des Martyrs, CS 20156, 38042 Grenoble cedex 9, France*

(Received 9 December 2016; published 1 February 2017)

The atomic-scale structure of aerodynamically levitated and laser-heated liquid tricalcium aluminate ($Ca_3Al_2O_6$) was measured at 2073(30) K by using the method of neutron diffraction with Ca isotope substitution (NDIS). The results enable the detailed resolution of the local coordination environment around calcium and aluminum atoms, including the direct determination of the liquid partial structure factor, $S_{CaCa}(Q)$, and partial pair distribution function, $g_{CaCa}(r)$. Molecular dynamics (MD) simulation and reverse Monte Carlo (RMC) refinement methods were employed to obtain a detailed atomistic model of the liquid structure. The composition $Ca_3Al_2O_6$ lies at the CaO-rich limit of the $CaO:Al_2O_3$ glass-forming system. Our results show that, although significantly depolymerized, liquid $Ca_3Al_2O_6$ is largely composed of AlO_4 tetrahedra forming an infinite network with a slightly higher fraction of bridging oxygen atoms than expected for the composition. Calcium-centered polyhedra exhibit a wide distribution of four- to sevenfold coordinated sites, with higher coordinated calcium preferentially bonding to bridging oxygens. Analysis of the MD configuration reveals the presence of ~10 % unconnected AlO_4 monomers and Al_2O_7 dimers in the liquid. As the CaO concentration increases, the number of these isolated units increases, such that the upper value for the glass-forming composition of $CaO:Al_2O_3$ liquids could be described in terms of a percolation threshold at which the glass can no longer support the formation of an infinitely connected AlO_4 network.

DOI: 10.1103/PhysRevB.95.064203

I. INTRODUCTION

Unlike pure silica SiO_2, liquid alumina Al_2O_3 does not form a glass. This is attributed to the observation that it does not satisfy Zachariasen's rules [1], because a significant fraction of aluminum atoms have a coordination number in excess of four and share edges [2]. However, the introduction of CaO increases the O:Al ratio and enables the formation of corner-shared AlO_4 tetrahedra that facilitate glass formation [3]. Liquid calcium aluminates are important components of natural magmas and are the precursors for solid materials with high thermal and chemical stabilities, that have wide application in aluminous cements [4], bioceramics [5,6], and infrared-transmitting glass optics [7–9]. A detailed and accurate description of the atomic-scale structure of these refractory liquids and the structural role of aluminum and calcium in them is, therefore, important to further our understanding of the behavior and rheology of magmas and the mechanisms of crystal nucleation and vitrification. This information is useful in order to improve the design and fabrication of functional glassy and ceramic materials. High-quality *in situ* measurements are important because they provide a rigorous test of the reliability of computer models calculated by molecular dynamics (MD) simulations. However, experiments on molten aluminates are particularly challenging due to the difficulty of containing liquids with melting points in excess of 2000 K. Also, the disordered nature of liquids and the considerable complexity of their constituent atom-atom correlations makes it inherently difficult to characterize their atomic-scale structure.

Containerless techniques, such as aerodynamic levitation with laser heating, eliminate physical contact and deleterious chemical reactions between the liquid and the sample-environment. This provides several key advantages over conventional furnace methods, including the ability to heat to temperatures well in excess of 2000 K and, by avoiding heterogeneous nucleation, to allow liquids to be supercooled to form novel glasses over a wide composition range. In a conventional furnace, glasses in the $(CaO)_x(Al_2O_3)_{1-x}$ system can be formed in a narrow composition range close to the eutectic composition ($x = 0.64$) [10]. Levitation techniques enable the extension of the glass-forming region to $0.46 \leqslant x \leqslant 0.75$ [11], where tricalcium aluminate ($Ca_3Al_2O_6$) represents the CaO-rich glass end-member at $x = 0.75$. The local aluminum coordination environment can be determined in this three-component system by using conventional neutron and x-ray diffraction combined with aerodynamic levitation methods [12,13]. However, it is difficult to determine the local calcium environment since the Ca-O correlations overlap considerably with the other atom-atom interactions and the Ca-Ca interactions are unresolvable [13]. It is therefore desirable to employ Ca-atom selective methods in order to

*james.drewitt@bristol.ac.uk

determine accurately the local calcium environment in these high-temperature levitated liquids.

Nuclear magnetic resonance (NMR) spectroscopy experiments using the quadrupolar spin-$\frac{7}{2}$ ^{43}Ca nuclide are limited by its low natural abundance and low sensitivity, as well as being particularly challenging at high temperature. The low energy of the absorption K edge for Ca at 4.0381 keV limits the maximum accessible scattering vector Q to about 4 Å^{-1} for anomalous x-ray scattering measurements, leading to poor resolution in real space. X-ray absorption spectroscopy measurements are also difficult to make on the small spherical samples used in levitation due to their sensitivity to the illuminated sample volume which can fluctuate with changing incident x-ray energy. In contrast, the method of neutron diffraction with isotope substitution (NDIS [14]) with Ca isotopes is a powerful approach to resolve the individual calcium atom-pair correlations in liquids and glasses. Levitation is well suited for *in situ* liquid NDIS measurements because it provides clean data sets requiring minimal background corrections. However, NDIS requires good counting statistics due to the sample sizes (∼2–3 mm diameter) and is thus limited by the available flux at neutron sources. NDIS has previously been used to measure the full set of partial structure factors of levitated liquid and supercooled $Ni_{36}Zr_{64}$ [15] and Ni-Si alloys [16], although these measurements benefit from the large scattering length contrast of 23.1 fm between the ^{58}Ni and ^{62}Ni isotopes.

Natural calcium is composed mainly of ^{40}Ca (96.941% abundance) and ^{44}Ca (2.086% abundance) that have coherent neutron-scattering lengths of 4.80(2) fm and 1.42(6) fm, respectively [17]. Although ^{43}Ca has a favorable negative scattering length [−1.56(9) fm], its low abundance (0.135%) means that it is generally impractical to use it for NDIS experiments. Hence, mixtures of calcium in its natural abundance and ^{44}Ca are commonly used in NDIS experiments providing a modest scattering length contrast of 3.28(4) fm. NDIS with Ca isotopes was used previously to determine $S_{\mathrm{CaCa}}(Q)$ in $(CaO)_{0.48}(SiO_2)_{0.49}(Al_2O_3)_{0.03}$ glass [18,19], and has been combined with aerodynamic levitation and laser heating to investigate the structure of liquid and glassy $CaSiO_3$ [20] and $CaAl_2O_4$ [3]. The latter experiments enabled the successful precise determination of the Ca-O coordination environment in these liquids, and although the $S_{\mathrm{CaCa}}(Q)$ was indiscernible for the liquid above the statistical noise, $S_{\mathrm{CaCa}}(Q)$ was successfully determined for the $CaAl_2O_4$ glass [3].

In this paper, we present the results of a NDIS experiment of aerodynamically levitated and laser-heated liquid $Ca_3Al_2O_6$ at 2073(30) K. The measurements are of suitable statistical precision to enable the accurate determination of the local coordination environment around calcium and aluminium atoms, including the direct determination of the liquid $S_{\mathrm{CaCa}}(Q)$ partial structure factor. The results are discussed by comparison to a structural model determined from molecular dynamics (MD) simulations employing advanced polarizable ion model potentials [13]. This MD structural model was further refined by using the reverse Monte Carlo (RMC) simulation method to identify the origin of subtle differences between the experimental and simulation results.

II. THEORY

In a neutron-diffraction measurement for a liquid, the coherent scattered intensity is represented by the total structure factor

$$F(Q) = \sum_{\alpha}\sum_{\beta} c_\alpha c_\beta b_\alpha b_\beta [S_{\alpha\beta}(Q) - 1], \tag{1}$$

where $S_{\alpha\beta}(Q)$ is a Faber–Ziman [21] partial structure factor for chemical species α and β, Q is the magnitude of the scattering vector, c_α and c_β denote the atomic fractions of chemical species α and β, and b_α and b_β denote their coherent neutron-scattering lengths. In this work three structurally identical samples of $Ca_3Al_2O_6$ were prepared by using either Ca in its natural isotopic abundance, predominantly ^{44}Ca, and a 50 : 50 mixture of the two. Due to the contrast in scattering lengths of the different calcium isotopes, the $S_{\alpha\beta}(Q)$ functions containing Ca receive different weightings and give rise to observably different total structure factors denoted $^{\mathrm{nat}}F(Q)$, $^{\mathrm{mix}}F(Q)$, and $^{44}F(Q)$.

By linear combination of these $F(Q)$ it is possible to eliminate certain partial structure factors from the scattering function. A particularly useful decomposition is to consider the pseudobinary combination which, from Eq. (1), we write as

$$F(Q) = c_{\mathrm{Ca}}^2 b_{\mathrm{Ca}}^2 [S_{\mathrm{CaCa}}(Q) - 1] + 2c_{\mathrm{Ca}} b_{\mathrm{Ca}} \delta_{\mathrm{Ca}\mu}(Q) + \delta_{\mu\mu}(Q), \tag{2}$$

where

$$\delta_{\mathrm{Ca}\mu}(Q) = c_{\mathrm{Al}} b_{\mathrm{Al}} [S_{\mathrm{CaAl}}(Q) - 1] + c_{\mathrm{O}} b_{\mathrm{O}} [S_{\mathrm{CaO}}(Q) - 1], \tag{3}$$

and

$$\begin{aligned}\delta_{\mu\mu}(Q) = {} & c_{\mathrm{Al}}^2 b_{\mathrm{Al}}^2 [S_{\mathrm{AlAl}}(Q) - 1] + c_{\mathrm{O}}^2 b_{\mathrm{O}}^2 [S_{\mathrm{OO}}(Q) - 1] \\ & + 2c_{\mathrm{Al}} c_{\mathrm{O}} b_{\mathrm{Al}} b_{\mathrm{O}} [S_{\mathrm{AlO}}(Q) - 1].\end{aligned} \tag{4}$$

Here $S_{\mathrm{CaCa}}(Q) - 1$ is a direct measure of the Ca-Ca partial structure factor, $\delta_{\mathrm{Ca}\mu}(Q)$ is a structure factor that contains all correlations with Ca apart from with itself and $\delta_{\mu\mu}(Q)$ is a structure factor that does not contain any Ca correlations.

We can express these combinations in matrix form as

$$\begin{bmatrix} {}^{44}F(Q) \\ {}^{\mathrm{mix}}F(Q) \\ {}^{\mathrm{nat}}F(Q) \end{bmatrix} = [A] \begin{bmatrix} S_{\mathrm{CaCa}}(Q) - 1 \\ \delta_{\mathrm{Ca}\mu}(Q) \\ \delta_{\mu\mu}(Q) \end{bmatrix}, \tag{5}$$

where

$$[A] = \begin{bmatrix} c_{\mathrm{Ca}}^2 b_{44}^2 & 2c_{\mathrm{Ca}} b_{44} & 1 \\ c_{\mathrm{Ca}}^2 b_{\mathrm{mix}}^2 & 2c_{\mathrm{Ca}} b_{\mathrm{mix}} & 1 \\ c_{\mathrm{Ca}}^2 b_{\mathrm{nat}}^2 & 2c_{\mathrm{Ca}} b_{\mathrm{nat}} & 1 \end{bmatrix}. \tag{6}$$

Hence from Eq. (5) we can write

$$\begin{bmatrix} S_{\mathrm{CaCa}}(Q) - 1 \\ \delta_{\mathrm{Ca}\mu}(Q) \\ \delta_{\mu\mu}(Q) \end{bmatrix} = [A]^{-1} \begin{bmatrix} {}^{44}F(Q) \\ {}^{\mathrm{mix}}F(Q) \\ {}^{\mathrm{nat}}F(Q) \end{bmatrix}. \tag{7}$$

Using the values $b_{\mathrm{nat}} = 0.470(2)$, $b_{44} = 0.164(6)$, and $b_{\mathrm{mix}} = 0.317(3) \times 10^{-1}$ fm, for the isotopic combinations used in this work, and $b_{\mathrm{Al}} = 0.3449(5)$ and $b_{\mathrm{O}} = 0.5803(4) \times 10^{-1}$ fm

[17], we find

$$[A]^{-1} = \begin{bmatrix} 287.164 & -574.328 & 287.164 \\ -30.818 & 49.653 & -18.835 \\ 3.182 & -3.293 & 1.110 \end{bmatrix}.$$

It is also useful, as a check, to calculate from $^{\text{nat}}F(Q)$ and $^{44}F(Q)$ alone, the first-order difference functions

$$\begin{aligned} \Delta_{\text{Ca}}(Q) &\equiv {}^{\text{nat}}F(Q) - {}^{44}F(Q) \\ &= c_{\text{Ca}}^2\left(b_{\text{nat}}^2 - b_{44}^2\right)[S_{\text{CaCa}}(Q) - 1] \\ &\quad + 2c_{\text{Ca}}(b_{\text{nat}} - b_{44})\delta_{\text{Ca}\mu}(Q), \end{aligned} \tag{8}$$

and

$$\Delta_{\mu\mu}(Q) = \delta_{\mu\mu}(Q) - c_{\text{Ca}}^2 b_{\text{nat}} b_{44}[S_{\text{CaCa}}(Q) - 1], \tag{9}$$

which are independent of the measurement of $^{\text{mix}}F(Q)$.

In real space, the total pair distribution function $G(r)$ provides a measure of probability of finding two atoms a distance r apart and is determined by the Fourier transformation

$$\begin{aligned} G(r) &= \frac{1}{2\pi^2 r\rho}\int_0^\infty Q[F(Q)]\sin(Qr)dQ \\ &= \sum_{\alpha=1}^{n}\sum_{\beta=1}^{n} c_\alpha c_\beta b_\alpha b_\beta [g_{\alpha\beta}(r) - 1], \end{aligned} \tag{10}$$

where ρ denotes the atomic number density, and $g_{\alpha\beta}(r)$ is a partial pair distribution function. The mean coordination number $\bar{n}_\alpha^\beta$ gives the average number of β atoms in a spherical coordination shell of radius $r_1 \leqslant r \leqslant r_2$ centered on an atom of type α and is obtained by integrating over a peak in real space arising from a specific $g_{\alpha\beta}(r)$ function, according to

$$\bar{n}_\alpha^\beta = 4\pi\rho c_\beta \int_{r_1}^{r_2} g_{\alpha\beta}(r) r^2 dr. \tag{11}$$

The real-space difference functions, denoted $\delta G_{\text{Ca}\mu}(r)$, $\delta G_{\mu\mu}(r)$, $\Delta G_{\text{Ca}}(r)$, and $\Delta G_{\mu\mu}(r)$, are obtained by Fourier transforming the corresponding reciprocal-space functions in Eqs. (3), (4), (8), and (9), respectively, and are defined by replacing the $S_{\alpha\beta}(Q)$ functions by their corresponding real-space partials $g_{\alpha\beta}(r)$.

III. EXPERIMENTAL METHOD

A. Sample preparation

Three samples corresponding to $^{\text{nat}}F(Q)$, $^{\text{mix}}F(Q)$, and $^{44}F(Q)$ were prepared by weighing powders, in the correct proportions, of Al_2O_3 ($\geqslant$99.9%) and $^{\text{nat}}CaCO_3$ or $^{44}CaCO_3$ (97% enrichment) mixed with $^{44}CaAl_2O_4$ glass (99.2% enrichment) prepared for a previous experiment [3]. Each sample was melted in a platinum crucible by using the method described in Ref. [22]. The resulting polycrystalline ceramics were levitated on a stream of 96.5% Ar + 3.5% O_2 (Arcal 22, Air Liquide) gas and melted by CO_2 laser heating. After rapid cooling, by switching off the laser power, spherical glasses were formed with diameters of 2.64(1) mm for the $^{\text{nat}}$Ca sample and 2.40(1) mm for the ^{44}Ca and $^{\text{mix}}$Ca samples. Sample reproducibility was checked by unpolarized Raman spectra measured for the glass samples at room temperature by using a T64000 Jobin Yvon confocal micro-Raman spectrometer equipped with a CCD detector with the 514.532 nm line of a Coherent Ar^+ laser as the excitation source. The spectra are consistent with previous Raman measurements of $Ca_3Al_2O_6$ glass [11,22], exhibiting a strong band at 756 cm^{-1}, attributed to a symmetric vibration of Q^2 species, and a medium-intensity band at 560 cm^{-1}.

B. Neutron-diffraction measurements

The neutron-diffraction measurements were made using the D4c neutron diffractometer [23] at the Institut Laue–Langevin operating at an incident wavelength of 0.4979(1) Å, giving a Q range of $0.3 \leqslant Q\,(\text{Å}^{-1}) \leqslant 23.45$. The experiments on the liquids were made by using the aerodynamic levitation device described in Ref. [24]. To reduce the background scattering, the upper section of the conical nozzle was manufactured out of vanadium, which scatters neutrons almost entirely incoherently. Furthermore, neutron-absorbing $^{10}B_4C$ slits collimated to around 5 mm vertically by 10 mm horizontally at the sample position were positioned close to the nozzle to mask it from the incident neutron beam. The samples were heated above their melting point by using two 125 W CO_2 lasers pointing downwards onto the sample at an angle of 20° to the vertical in order to achieve a homogeneous temperature distribution. The temperature was monitored by using an optical pyrometer operating at a wavelength of 0.85 μm pointing at the upper surface of the sample. Diffraction patterns were measured for the liquid samples levitated on a stream of 96.5% Ar + 3.5% O_2 (Arcal 22, Air Liquide) gas at 2073(30) K, for the empty levitation chamber inside the diffraction chamber with a flow of gas, and a solid vanadium sphere of 3 mm diameter for normalization purposes. Counting times were approximately 20 h for the $^{\text{nat}}$Ca and ^{44}Ca liquids and 40 h for the $^{\text{mix}}$Ca. For each set of measurements, successive diffraction patterns were compared and no deviation was found outside the statistical noise. The measured background intensity was relatively small, originating predominantly from gas scattering in the chamber, and extremely stable: we observed no change in background intensity outside of statistical error during the course of the experiment. The mean temperature of the samples remained stable throughout the measurements, with only small periodic variations of ±30 K due to sample rotation. The samples were weighed before and after the experiment and no mass loss was observed. The measured data sets were corrected by using the methodology described in Ref. [14], with sample attenuation factors calculated for spherical sample geometry [25]. Each data set was checked for self-consistency by ensuring that the back-Fourier transform of the corresponding real-space functions, after the region below the first interatomic distance is set to the theoretical $r = 0$ limit, was in good overall agreement with the original reciprocal-space measurements [26].

C. Simulation methods

Molecular dynamics simulations were performed by using an advanced ionic interaction potential that is built on formal charges [27]. It includes Coulomb and dispersion interactions and electric polarization effects up to the quadrupolar level. Anions are considered compressible and deformable. The

potential parameters for the Ca-Al-O system studied here have been optimized by reference to electronic structure calculations [13,27]. The simulation cell of $Ca_3Al_2O_6$ liquid contained 1892 ions (1032 O^{2-}, 344 Al^{3+}, and 516 Ca^{2+}). MD simulations were performed with a time step of 1 fs at a constant temperature of 2500 K and constant density. Temperature was controlled by a Nose–Hoover thermostat [28]. At ambient pressure and 2500 K, the potential predicts an atomic number density of 0.0632 Å^{-3}, which is very similar to the experimental value of $\rho = 0.0655$ Å^{-3} at 2073 K [29,30]. Additional simulations made at the experimental density did not lead to significant changes in the structure of the liquid. Structural properties such as pair distribution functions, structure factors and coordination numbers were derived from MD trajectories of 50 ps simulation time taken after 50 ps equilibration time. Convergence of the obtained structure information was confirmed by averaging over different time intervals.

The structural model obtained from the MD simulations was refined by reverse Monte Carlo (RMC) methods using the program RMCPROFILE [31] (version 6). The RMC refinement was run with steps of 0.05 Å until the overall χ^2 fit approached a constant value. The analysis and presentation of the refined data was carried out by averaging the results of 5 RMC refinements from the original MD configuration.

IV. RESULTS

A. Neutron diffraction

The measured total structure factors $^{nat}F(Q)$, $^{mix}F(Q)$, and $^{44}F(Q)$ for liquid $Ca_3Al_2O_6$ at 2073(30) K are shown in Fig. 1. The results show the progressive appearance of a prepeak at $Q \approx 1.5$ Å^{-1} as natural Ca is substituted by ^{44}Ca; a feature which is indicative of ordering on an intermediate length scale for many liquids and glasses [33]. Systematic variations in the relative intensities of the principal peak at $Q \approx 2.7$ Å^{-1}, the second peak at $Q \approx 4.6$ Å^{-1}, and the broad doublet feature with a centroid at $Q \approx 8$ Å^{-1}, are also observed between the isotopically substituted samples. For comparison, the high-energy x-ray structure factor $S_X(Q)$ for liquid $Ca_3Al_2O_6$ at 2273(30) K from Ref. [13] is shown in Fig. 2(a). The $S_X(Q)$ function exhibits a peak at 2.19(2) Å^{-1} arising from cation-cation correlations [13]. This peak is absent in the corresponding neutron structure factor due to the lower neutron-scattering cross sections for the cations compared with x-ray scattering.

The total pair distribution functions $^{nat}G(r)$, $^{mix}G(r)$, and $^{44}G(r)$ obtained by Fourier transforming the corresponding $F(Q)$ functions are shown in Fig. 3. The first peak in the $G(r)$ functions is assigned to the nearest-neighbor Al-O correlations and its position gives a bond length of $r_{AlO} = 1.75(1)$ Å in all three measurements. A coordination number $\bar{n}^{O}_{Al} = 4.4(2)$ was determined from the area of the Al-O peak in $^{nat}G(r)$ up to the first minimum by using Eq. (11), while a value $\bar{n}^{O}_{Al} = 4.3(2)$ was determined by integrating over the Al-O peak in $^{mix}G(r)$ and $^{44}G(r)$. This difference in $\bar{n}^{O}_{Al}$ is attributed to a stronger overlap into the Al-O coordination shell by Ca-O correlations which gives rise to a peak in $^{nat}G(r)$ at $r_{CaO} = 2.36(3)$ Å. Due to the progressive reduction in the neutron-scattering length of calcium, the Ca-O correlations give rise to a weaker peak in $^{mix}G(r)$ at $r_{CaO} = 2.30(5)$ Å and become indiscernible in $^{44}G(r)$. The measured bond lengths r_{AlO}, r_{CaO}, r_{CaCa} and average coordination numbers $\bar{n}^{O}_{Al}$, $\bar{n}^{O}_{Ca}$, $\bar{n}^{Ca}_{Ca}$ determined from the real-space results are listed in Table I.

As in previous studies of calcium aluminate liquids and glasses, where the coordination number $\bar{n}^{O}_{Ca}$ was obtained either by direct integration or by fitting a symmetric Gaussian function [12,13,34–36], we find that integration over the region of the Ca-O peak results in a significant underestimate in $\bar{n}^{O}_{Ca} \approx 4$. The position of the first peak in $G_X(r)$ from Ref. [13] [see Fig. 3(b)] gives $r_{AlO} = 1.78(1)$ Å and $\bar{n}^{O}_{Al} = 4.3(1)$, while the second peak gives $r_{CaO} = 2.30(3)$ and $\bar{n}^{O}_{Ca} = 4.0(5)$. The

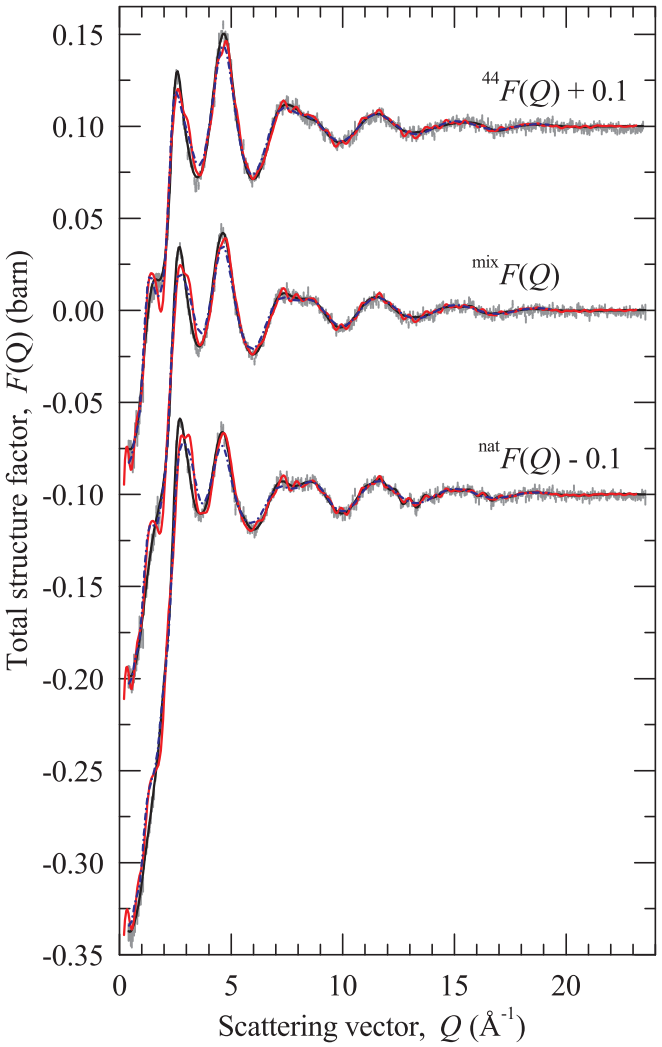

FIG. 1. Total structure factors $^{44}F(Q)$, $^{mix}F(Q)$, and $^{nat}F(Q)$ measured by neutron diffraction for the aerodynamically levitated $Ca_3Al_2O_6$ liquids at 2073(30) K. The vertical bars show the statistical errors and the solid dark-black curves are the Fourier back-transforms of the corresponding total pair distribution $G(r)$ functions shown in Fig. 3 after the region below the first interatomic distance was set to the theoretical $r = 0$ limit. The chained blue curves show the functions generated from the MD simulations and the solid light-red curves show the results of the RMC structural refinement. For clarity, the results are displaced vertically.

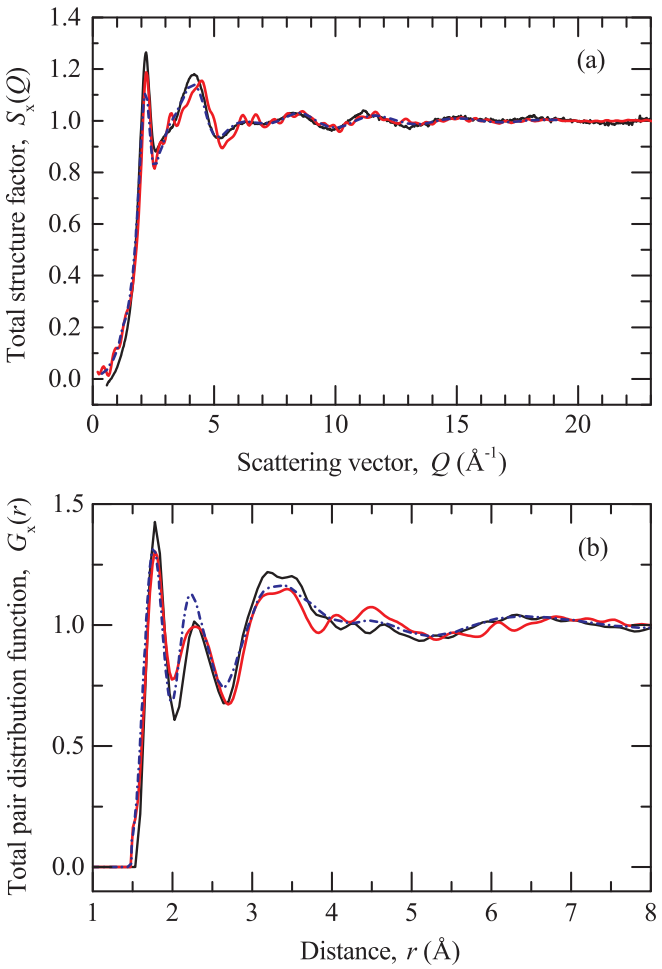

FIG. 2. The measured high-energy x-ray (a) structure factor $S_X(Q)$ and (b) pair distribution function $G_X(r)$ for liquid $Ca_3Al_2O_6$ at 2273(30) K (solid dark-black curves) together with the corresponding functions obtained from the MD simulations (chained blue curve) and the results of the RMC structural refinement (solid light-red curve).

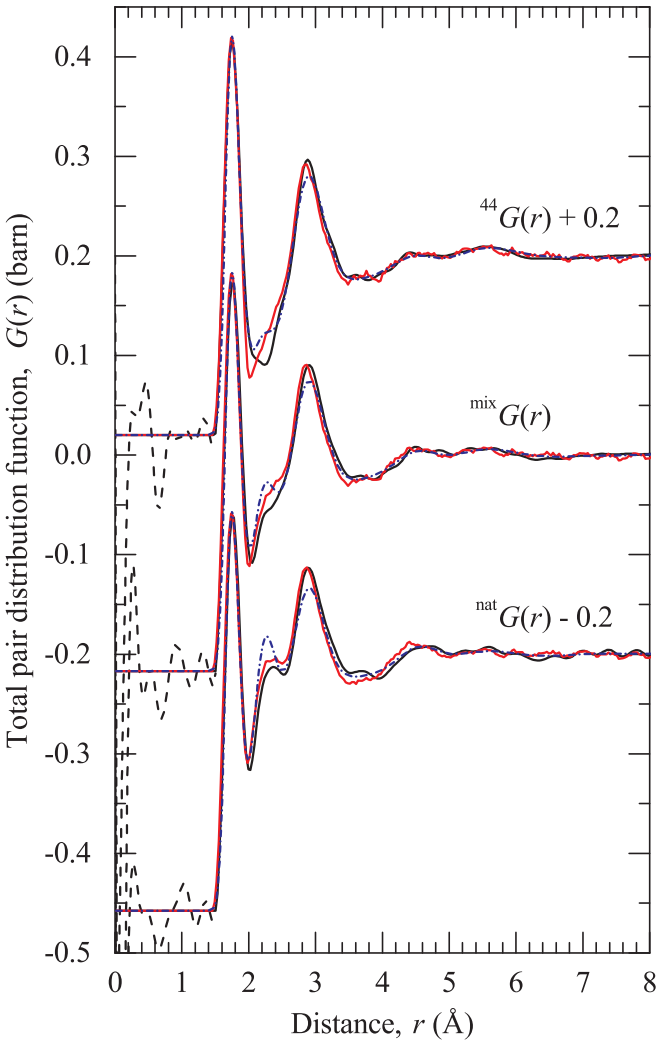

FIG. 3. The total pair distribution functions $^{44}G(r)$, $^{mix}G(r)$, and $^{nat}G(r)$ for liquid $Ca_3Al_2O_6$ at 2073(30) K (solid dark black curves), as obtained by Fourier transforming the corresponding total structure factors given in Fig. 1 after making a spline fit to the data and applying a cosine window function [32] between $20 \leqslant Q$ (Å^{-1}) $\leqslant 23.55$. The broken black curves show the extent of the unphysical low-r features, the chained blue curves are the functions generated directly from the MD simulations, and the solid light-red curves show the results of the RMC structural refinement. For clarity, the results are displaced vertically.

underestimate in $\bar{n}^{O}_{Ca}$ seen by both neutron and x-ray diffraction measurements is due to the strong overlap of the Ca-O peak by O-O correlations which obscures Ca-O correlations at higher r [13].

The reciprocal-space difference functions $\delta_{\mu\mu}(Q)$, $\Delta_{\mu\mu}(Q)$, $\Delta_{Ca}(Q)$, and $\delta_{Ca\mu}(Q)$, and corresponding real-space functions $\delta G_{\mu\mu}(r)$, $\Delta G_{\mu\mu}(r)$, $\Delta G_{Ca}(r)$, and $\delta G_{Ca\mu}(r)$, are shown in Figs. 4 and 5, respectively. All correlations involving Ca have been eliminated in $\delta_{\mu\mu}(Q)$ and $\Delta_{\mu\mu}(Q)$, leaving only μ-μ (μ = Al,O) contributions. The first peak in $\delta G_{\mu\mu}(r)$ and $\Delta G_{\mu\mu}(r)$ at $r_{AlO} = 1.75(1)$ Å arises from the nearest-neighbor Al-O correlations. Integration over this peak up to 2.0 Å gives $\bar{n}^{O}_{Al} = 4.1(1)$ and 4.2(1), respectively. In the $\Delta G_{Ca}(r)$ and $\delta G_{Ca\mu}(r)$ functions, all μ-μ correlations have been eliminated, and the first peak assigned to Ca-O correlations at $r_{CaO} = 2.29(2)$ Å and 2.26(2) Å, respectively, is clearly resolved extending to $r \sim 3$ Å. Integrating over the Ca-O peak up to 3 Å in $\Delta G_{Ca}(r)$ and $\delta G_{Ca\mu}(r)$ gives a coordination number $\bar{n}^{O}_{Ca} = 5.7(2)$. Although the difference functions allow for a much clearer resolution of the Al-O and Ca-O peaks compared with the total $G(r)$ functions, the associated partials $g_{AlO}(r)$ and $g_{CaO}(r)$ are not entirely isolated, such that the value of the coordination number is dependent on the integration cutoff value (see Fig. 6), especially at higher r where contributions from the correlations of other atomic pairs become more significant.

The measured partial structure factor $S_{CaCa}(Q)$ and the partial pair distribution function $g_{CaCa}(r)$ for liquid $Ca_3Al_2O_6$ are shown in Fig. 7. The $S_{CaCa}(Q)$ exhibits a weak diffraction peak at 1.2(1) Å^{-1} and a principal peak at 2.2(1) Å^{-1}. The position of the first peak in $g_{CaCa}(r)$ gives a Ca-Ca bond distance of $r_{CaCa} = 3.62(4)$ Å. Integration over this peak up to 5.03 Å gives an average coordination number $\bar{n}^{Ca}_{Ca} = 7.9(5)$.

TABLE I. Measured real-space peak positions r_{AlO}, r_{CaO}, r_{CaCa}, and coordination numbers $\bar{n}^{O}_{Al}$, $\bar{n}^{O}_{Ca}$, $\bar{n}^{Ca}_{Ca}$ for liquid $Ca_3Al_2O_6$, together with the results from molecular dynamics (MD) and reverse Monte Carlo (RMC) simulations.

Function	r_{AlO} (Å)	r_{CaO} (Å)	r_{CaCa} (Å)	$\bar{n}^{O}_{Al}$	$\bar{n}^{O}_{Ca}$	$\bar{n}^{Ca}_{Ca}$
$^{nat}G(r)$	1.75(1)	2.36(3)		4.4(2)	4.0(5)	
$^{mix}G(r)$	1.75(1)	2.30(5)		4.3(2)	4.0(5)	
$^{44}G(r)$	1.75(1)			4.3(2)		
$G_X(r)$	1.78(1)	2.30(3)	3.49(5)	4.3(2)	4.0(5)	
$\delta G_{\mu\mu}(r)$	1.75(1)			4.1(1)		
$\Delta G_{\mu\mu}(r)$	1.75(1)			4.2(1)		
$\Delta G_{Ca}(r)$		2.29(2)			5.7(2)	
$\delta G_{Ca\mu}(r)$		2.26(2)			5.7(2)	
$g_{CaCa}(r)$			3.62(4)			7.9(5)
MD	1.75(1)	2.29(1)	3.65(3)	4.04(5)	5.62(5)	8.5(1)
RMC	1.75(1)	2.23(1)	3.6(1)	3.98(5)	5.73(5)	8.7(2)

B. Molecular dynamics simulations

The results from the MD simulations of liquid $Ca_3Al_2O_6$ at 2500 K are in good overall agreement with the experimentally measured functions shown in Figs. 1 to 7, suggesting that interpretation of the MD configurations and dynamics should give a good representation of the atomistic structure and dynamics of liquid $Ca_3Al_2O_6$. With the cutoff values defined by the first minimum in the respective $g_{\alpha\beta}(r)$ functions, the average Ca coordination by oxygen $\bar{n}^{O}_{Ca} = 5.62(5)$ is very close to the experimental value, while the Al coordination by oxygen $\bar{n}^{O}_{Al} = 4.04(5)$ is slightly smaller. The coordination number $\bar{n}^{Ca}_{Ca} = 8.5(1)$ agrees with the experimental measurement within the limits of uncertainty.

Although there is good agreement between the experimental data and the MD simulation, there are some regions of notable discrepancies in both the real r-space and reciprocal Q-space data. In Q space (Fig. 1) this can be seen as a much less prominent prepeak at ~1.5 Å^{-1} and a less intense first peak. After ~5 Å^{-1} there is almost perfect agreement with the data. In r space (Fig. 3), the simulation results lead to more intensity in the region of the Ca-O peak at ~2.3 Å, suggesting that the simulation is overestimating the strength of the nearest-neighbor Ca-O interactions. In contrast, the peak at ~3.0 Å appears less intense in the MD simulations compared with the experimental data. This region is dominated by the first peak in $g_{OO}(r)$ but also has a small contribution from $g_{CaAl}(r)$.

C. Reverse Monte Carlo structure refinement

To understand the discrepancies observed between the experimental and simulation results, the structural model obtained from the MD simulation was refined by RMC methods. The experimental data included in the refinement were $S_{CaCa}(Q)$, $\delta_{Ca\mu}(Q)$, $\delta_{\mu\mu}(Q)$ from the neutron-diffraction measurements and $S_X(Q)$ from x-ray diffraction [13]. The low-r cutoffs used in the refinement were obtained by reference to the MD simulation. In addition, real-space data [$^{nat}G(r)$] was included to avoid a "pileup" of bonds close to the cutoff distances, primarily in $g_{CaO}(r)$ [38]. The mean square displacement from the original atoms at the end of the refinement, averaged for all refinements, was 0.063, 0.164, and 0.021 Å for the O, Al, and Ca atoms, respectively. It is noticeable that there is a strong preference for the Al atoms to move in the refinement procedure compared with the O and Ca atoms. Figure 8 compares the original MD to the RMC refined partial pair distribution functions.

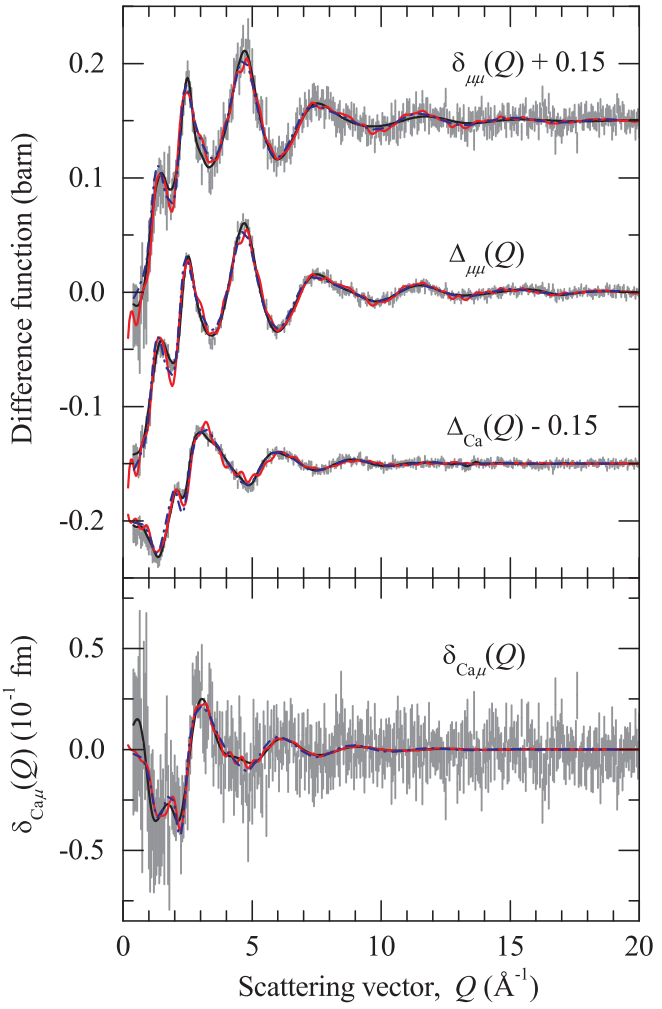

FIG. 4. The reciprocal-space difference functions $\delta_{\mu\mu}(Q)$, $\Delta_{\mu\mu}(Q)$, $\Delta_{Ca}(Q)$, and $\delta_{Ca\mu}(Q)$ for liquid $Ca_3Al_2O_6$. The vertical bars show the statistical errors arising from the experimental measurements, the solid dark black curves are the Fourier back-transforms of the corresponding real-space functions shown in Fig. 4 after the region below the first interatomic distance was set to the theoretical $r = 0$ limit, the chained blue curves show the difference functions calculated from the partial structure factors generated from the MD simulations, and the solid light-red curves are the results of the RMC structural refinement. For clarity, the results are displaced vertically.

The results presented in Fig. 3 show a decrease in height and shift to slightly lower r in the first peak in $g_{CaO}(r)$, bringing the intensity of $G(r)$ in the region corresponding to nearest-neighbor Ca-O interactions closer to the experimental measurement. However, the calculated $\bar{n}^{O}_{Ca}$ remains largely unchanged at 5.73(5) for the RMC configuration compared with 5.62(5) from the MD. This suggests that the structural changes are relatively subtle, with the RMC broadening the slightly-too-strong Ca-O interactions from the MD. The

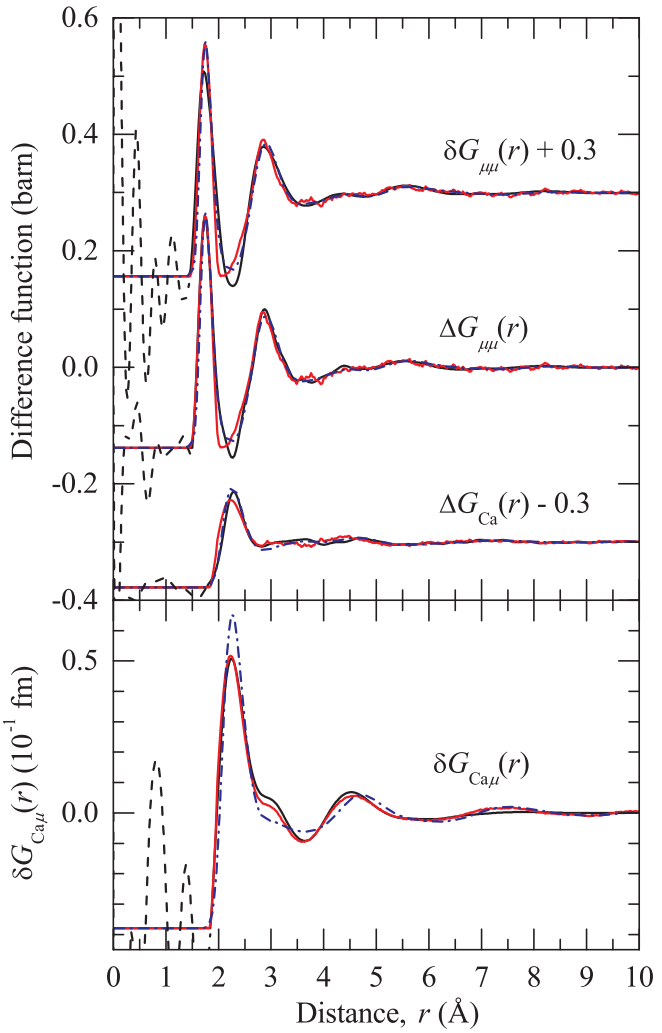

FIG. 5. The real-space difference functions $\delta G_{\mu\mu}(r)$, $\Delta G_{\mu\mu}(r)$, $\Delta G_{\mathrm{Ca}}(r)$, and $\delta G_{\mathrm{Ca}\mu}(r)$ for liquid $Ca_3Al_2O_6$ (solid dark-black curves), as obtained by Fourier transforming the corresponding reciprocal-space functions given in Fig. 4. The broken black curves show the extent of the unphysical low-r features, the chained blue curves show the functions calculated from the partial pair distribution functions generated directly from the MD simulations, and the solid light-red curves are the results of the RMC structural refinement. For clarity, the results are displaced vertically.

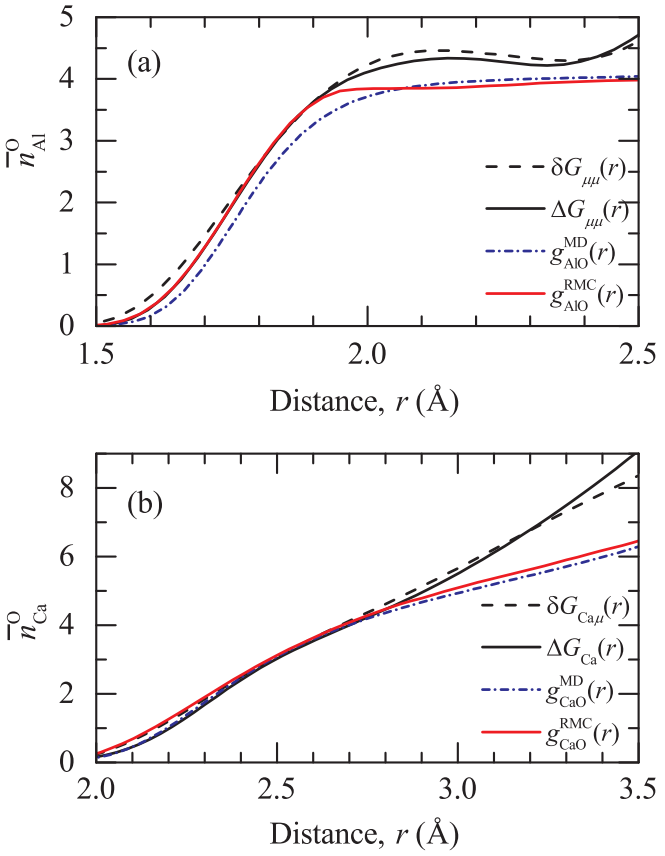

FIG. 6. Running coordination numbers (a) $\bar{n}^{O}_{Al}$ and (b) $\bar{n}^{O}_{Ca}$ determined from the measured difference functions and MD and RMC partial pair distribution functions indicated in the legend. The deviation at higher-r values is due to the contributions from correlations of other atomic pairs in the measured difference functions.

refinement also shows a sharpening and slight shift to low r in the first peak in $g_{\mathrm{AlO}}(r)$. The calculated coordination number $\bar{n}^{O}_{Al}$ from the RMC refinement gives 3.98(5) compared with a value of 4.04(5) for the MD simulation. Whereas $g_{\mathrm{OO}}(r)$ is virtually unchanged in the refinement, it is notable that the first peak $g_{\mathrm{CaAl}}(r)$ shifts to lower r and increases in intensity. Both $g_{\mathrm{AlAl}}(r)$ and $g_{\mathrm{CaCa}}(r)$ remain largely unchanged in the refinement procedure. Hence the higher peak at ~3 Å in the diffraction data (Fig. 3) is primarily due to the change in $g_{\mathrm{CaAl}}(r)$ observed in the refinement.

The bond-angle distributions show little change between the MD configuration and RMC refinement suggesting there is little difference in the topology of the two. The O-Al-O distribution is narrow and centered around 105°, confirming that the fourfold coordinated AlO_4 units are tetrahedral in nature. The O-O-O distribution shows a narrow peak at ~60° with a much wider peak centered around ~130° and is very similar to that observed in barium aluminate glass [20]. Overall, the RMC refinement made subtle changes to the MD configuration in order to achieve a better fit to the experimental data, but the basic structure is largely unchanged. From these results we consider that this combination of MD simulation and RMC refinement demonstrates that we have a good atomistic model of this liquid.

V. DISCUSSION

A. Aluminum network structure

The analysis of the MD and RMC configurations shows a structure largely composed of tetrahedrally coordinated AlO_4 units with ~93% fourfold coordinated aluminum atoms. Although this is a liquid in which the local structural configurations may be short lived (single Al-O bond lifetimes in the MD configuration are on the order of 20 ps), a suitable starting point for discussion of the aluminum network structure is in terms of the connection between AlO_4 tetrahedra. To form a perfectly connected network in which any two Al atoms are connected by a single bridging oxygen atom (BO), the Al : O ratio needs to be 1 : 2 precisely. For $(MO)_x(Al_2O_3)_{(1-x)}$ systems this ratio occurs precisely at $x = 0.5$. The $Ca_3Al_2O_6$

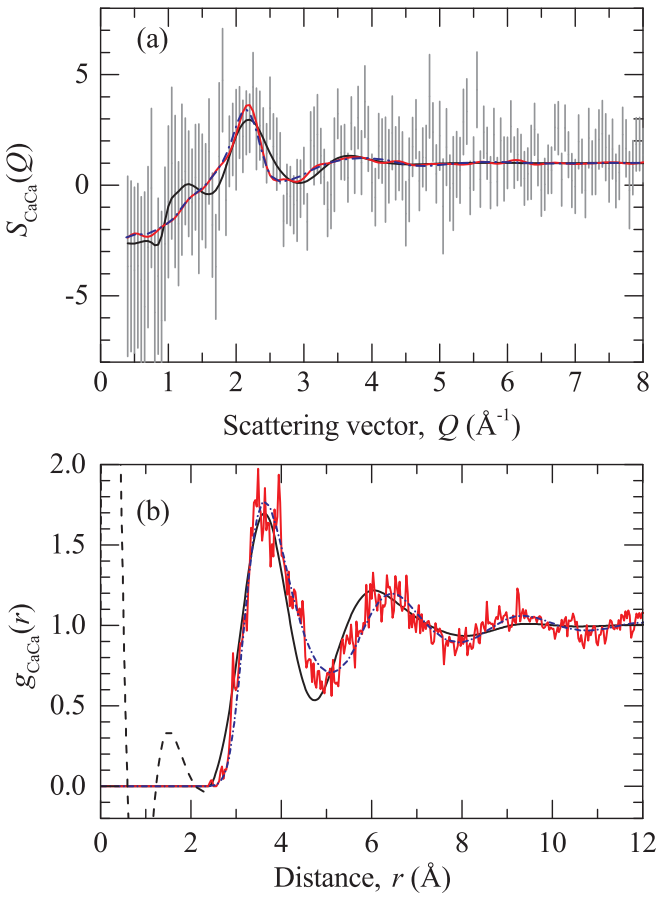

FIG. 7. (a) The partial structure factor $S_{CaCa}(Q)$ for liquid $Ca_3Al_2O_6$ as determined from the NDIS measurements (vertical error bars). The solid dark-black curve shows the Fourier back-transform of the experimental $g_{CaCa}(r)$ after the region below the first interatomic distance was set to the theoretical $g_{CaCa}(r = 0) = 0$ limit. (b) The partial pair distribution function $g_{CaCa}(r)$ as obtained by Fourier transforming the measured $S_{CaCa}(Q)$ shown in panel (a) after making a spline fit to the data and truncation at 8.0 Å^{-1} using a Lorch window function [37] (solid dark-black curve). The chained blue curves show the results generated directly from the MD simulations and the solid light-red curves show the RMC structural refinement.

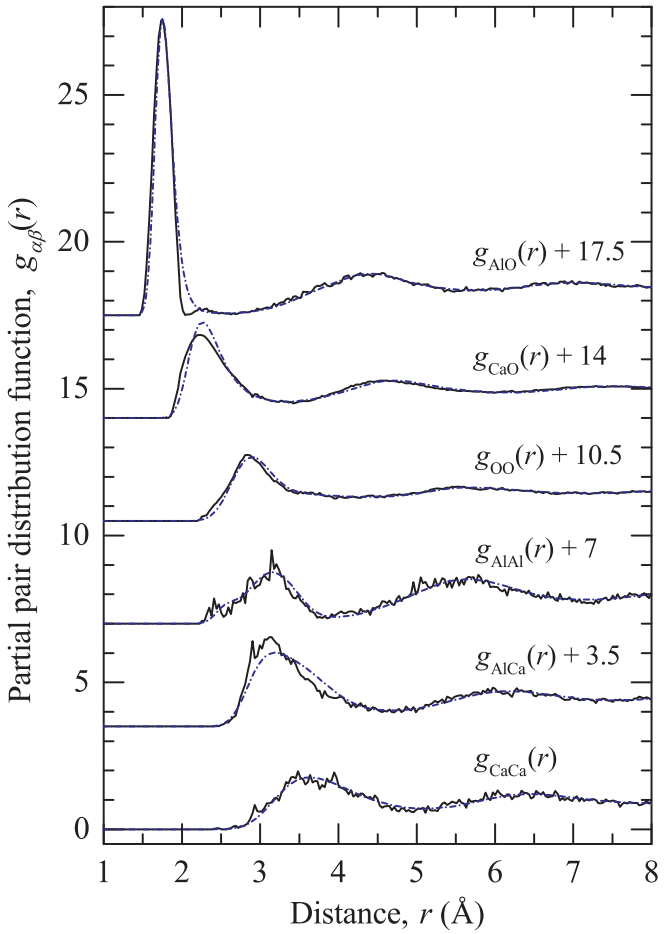

FIG. 8. The comparison of the partial pair radial distribution functions, $g_{\alpha\beta}(r)$, obtained from the MD simulation (chained blue curves) and after the RMC refinement of the MD configuration (solid black curves). For clarity, the results are displaced vertically.

system studied here corresponds to $x = 0.75$ and, provided there is no formation of oxygen triclusters (oxygen atoms connected to three tetrahedrally coordinated Al atoms), it is expected that, in this system, there will be a significant number of oxygen atoms that are connected to only one Al atom (nonbridging oxygen, NBO), as observed in $Ca_3Al_2O_6$ liquid and glass by spectroscopy techniques [22,39]. By using Eq. (1) in Skinner *et al.* [40], the mean number of bridging oxygens per Al atom in $Ca_3Al_2O_6$ is 2 and the fraction of NBO present should be 2/3, and BO should be 1/3. Analysis of the MD and the RMC refined data gives values of 60% and 36% for NBO and BO, respectively, which suggests there are slightly more bridging oxygens than expected from the simple network model. This difference is accounted for by 3%–4% "free oxygen" ions, which are not bonded to Al, and ~1% of O atoms in an oxygen tricluster. The fraction of "free oxygen" is similar to the value found in analogous silicate melts [41]. Analysis of the MD model shows that, although most of the AlO_4 tetrahedra belong to an infinitely connected major corner-shared cluster, around 15% to 20% Al are not connected to this largest network cluster with around 10% Al either forming Al_2O_7 dimers or isolated AlO_4 tetrahedral units (see Fig. 9).

B. The calcium coordination

Analysis of the simulation configurations show the calcium-centered polyhedra exhibit a wide distribution in four-,five-, six- and sevenfold coordinated sites with no preference for a particular Ca-O structural motif in the liquid. Calcium is coordinated on average by 5.62 oxygen atoms and all Ca-O polyhedra are connected by corners to a single network, with 90% Ca-O motifs exhibiting edge- and face-sharing connectivity. Calcium polyhedra with five- and sixfold coordination exhibit 25%–27% BO, 68%–69% NBO and 4%–5% "free" oxygen neighbors. A representative snapshot illustrating two calcium-centered polyhedra is shown in Fig. 10, in which each oxygen is connected to about four cations (Ca^{2+} or Al^{3+}) with free oxygens bonded to 4.2 Ca neighbors, NBOs bonded to 3.2 Ca neighbors (+1 Al), BOs bonded to 2.1 Ca neighbors

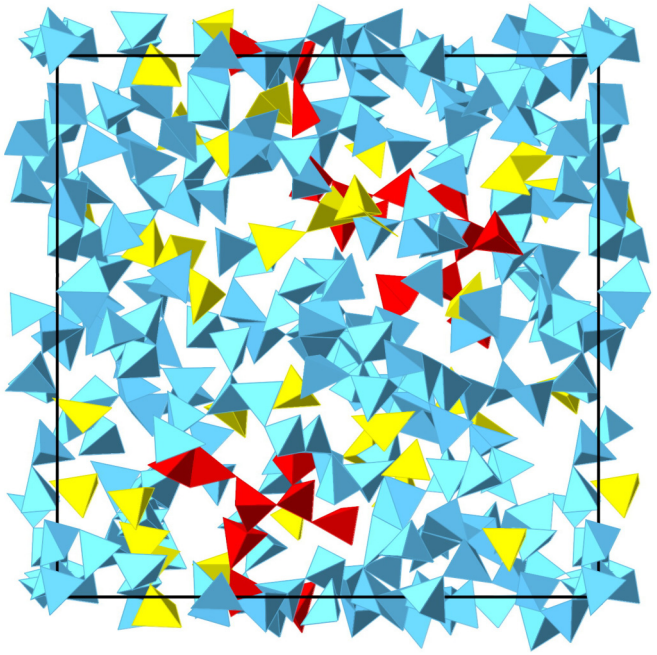

FIG. 9. The AlO_4 network structure in liquid $Ca_3Al_2O_6$ from the MD simulation at 2500 K. The blue tetrahedra represent the infinitely connected major cluster, with the red polyhedra showing two clusters with 11 and 12 connected tetrahedra and yellow polyhedra denoting the AlO_4 monomers and Al_2O_7 dimers.

(+2 Al), and tricluster oxygens bonded to 1.3 Ca neighbors (+3 Al).

Lower-coordinated calcium ions (2–4 fold coordination, about 10% of all Ca) have more NBO (76%) and fewer BO (19%) neighbors, while higher coordinated calcium ions with 7–8 oxygen neighbors (17% of all Ca) have a lower fraction of NBO (61%) and preferentially bond to a higher fraction of BO (35%) neighbors. The Ca-Ca coordination

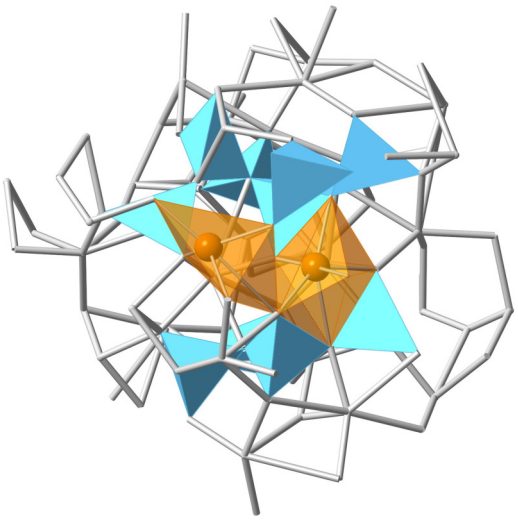

FIG. 10. Representative snapshot showing two (strongly distorted) calcium-centered polyhedra with coordination numbers of 5 and 6 (orange units). The blue units denote AlO_4 tetrahedra and the sticks represent oxygen-cation bonds.

does not depend on the Ca-O coordination and is constant at 8.5 (5.03 Å integration cutoff). The Ca-Al coordination increases steadily with increasing Ca-O coordination from 4.7 for fourfold coordinated Ca by oxygen, 5.0 for fivefold coordinated Ca, 5.4 for sixfold coordinated Ca, to 5.8 for sevenfold coordinated Ca by oxygen.

C. Glass-forming ability

The liquid $Ca_3Al_2O_6$ studied in this work lies on the CaO-rich limit at $x = 0.75$ of the $(CaO)_x(Al_2O_3)_{1-x}$ glass-forming system. As a highly viscous liquid, we would not expect a fully connected structure. However, although the liquid is significantly depolymerized, it possesses many of the structural characteristics required to form a glass network, including strong network-forming (AlO_4) motifs. As the liquid is quenched to form a glass we expect these AlO_4 motifs to remain and increase in their connectivity to ultimately form a continuously connected AlO_4 network that forms the basic glass structure. As this network forms we expect to see an increase in ordering in Ca-O correlations as the calcium is accommodated in the voids in the Al-O network.

Al_2O_3 does not form a glass by itself which may be explained simply as due to insufficient oxygen atoms being available to form a tetrahedrally connected AlO_4 network. When CaO is added to Al_2O_3 it increases the O:Al ratio while maintaining charge balance such that, at 50 : 50 CaO:Al_2O_3, enough oxygen atoms are present to form a fully connected Al-O tetrahedral network [3]. The calcium atoms then locate themselves in the voids between the tetrahedra. It appears that the size and charge of the Ca atoms is such that they do not put sufficient stress on the Al-O network to break it up. This would explain the beginning of the glass-forming region at around 50% CaO. This work shows that the further addition of CaO does not give rise to higher coordinated aluminum atoms but rather broadly maintains the AlO_4 motifs while increasing the number of NBO atoms in the network. As the number of NBO atoms increases, the rigidity and stability of the network will decrease, which would suggest a steady weakening of its glass-forming ability. However, the network may still, to a certain extent, be stabilized by the increased number of Ca atoms occupying voids in the network. Nevertheless, at some point it is expected that the continuity of the network will eventually break up. The composition of 75% CaO studied in this work appears to be this upper limit for the CaO:Al_2O_3 system. Our results demonstrate a significant number of unconnected AlO_4 monomers and Al_2O_7 dimers that do not belong to an infinitely connected cluster are already present. The number of these isolated units is expected to increase as the CaO content increases further. Indeed, we have carried out a further MD simulation at $x = 0.82$ which show that, by this composition, the maximum AlO_4 cluster size is less than 20 and is insufficient to support a fully connected network. In this way, the upper value for the glass composition could be described in terms of a percolation threshold at which the glass can no longer support the formation of an infinite Al-O cluster based on tetrahedral AlO_4 motifs. This could perhaps be studied further by a careful MD investigation based on topological constraint theory [42,43] at compositions close to the upper CaO limit of glass formation.

VI. CONCLUSIONS

In this work, we have applied the method of NDIS to successfully determine the local Ca coordination environment in liquid $Ca_3Al_2O_6$, which has been an obstacle in previous experimental studies of calcium-bearing oxide melts. Despite the relatively small scattering length contrast between the isotopes of Ca, our experimental measurements are of sufficient statistical precision to allow for the direct determination of the liquid $S_{CaCa}(Q)$ and $g_{CaCa}(r)$ partials. The combination of MD and RMC refinement simulation methods provides excellent agreement with the experimental data, demonstrating a reliable atomistic model of this liquid.

This composition is at the limit of the glass-forming region of $CaO{:}Al_2O_3$ glasses. The experimental confirmation of the atomistic structures obtained by MD simulations suggests that further MD simulations around this composition may give insight into its glass-forming region in terms of topological constraint theory.

The successful application of NDIS in a complex multicomponent oxide liquid paves the way for this technique to be applied to more chemically complex geological silicate melts [44]. A detailed understanding of the liquid structure of oxide melts at ambient pressure is an important prerequisite for interpreting the structural changes which occur at elevated temperatures and pressures experienced in planetary interiors [45]. The technique also allows for the determination of the local structure of other geologically important cations, such as Mg^{2+} or $Fe^{2+/3+}$, of which the local coordination environment in melts is not precisely known, even at ambient pressure.

ACKNOWLEDGMENTS

We thank Alain Bertoni for assistance with the neutron-diffraction experiments made at the Institut Laue–Langevin under proposal 6-05-956 [46]. The authors gratefully acknowledge the computing time granted by the John von Neumann Institute for Computing (NIC) and provided at Jülich Supercomputing Centre (JSC) under project ID HPO15.

[1] W. H. Zachariasen, J. Am. Chem. Soc. **54**, 3841 (1932).
[2] L. B. Skinner, A. C. Barnes, P. S. Salmon, L. Hennet, H. E. Fischer, C. J. Benmore, S. Kohara, J. K. Richard Weber, A. Bytchkov, M. C. Wilding, J. B. Parise, T. O. Farmer, I. Pozdnyakova, S. K. Tumber, and K. Ohara, Phys. Rev. B **87**, 024201 (2013).
[3] J. W. E. Drewitt, L. Hennet, A. Zeidler, S. Jahn, P. S. Salmon, D. R. Neuville, and H. E. Fischer, Phys. Rev. Lett. **109**, 235501 (2012).
[4] K. L. Scrivener, J. L. Cabiron, and R. Letourneux, Cem. Concr. Res. **29**, 1215 (1999).
[5] H. Engqvist, J.-E. Schultz-Walz, J. Loof, G. A. Botton, D. Mayer, M. W. Phaneuf, N.-O. Ahnfelt, and L. Hermansson, Biomaterials **25**, 2781 (2004).
[6] S.-H. Oh, S.-Y. Choi, Y.-K. Lee, and K. N. Kim, J. Biomed. Mater. Res. **62**, 593 (2002).
[7] J. E. Shelby, C. M. Shaw, and M. S. Spess, J. Appl. Phys. **66**, 1149 (1989).
[8] Y.-M. Sung and S.-J. Kwon, J. Mater. Sci. Lett. **18**, 1267 (1999).
[9] W. J. Chung and J. Heo, J. Am. Ceram. Soc. **84**, 348 (2001).
[10] P. L. Higby, R. J. Ginther, I. D. Aggarwal, and E. J. Friebele, J. Non-Cryst. Solids **126**, 209 (1990).
[11] M. Licheron, V. Montouillout, F. Millot, and D. R. Neuville, J. Non-Cryst. Solids **357**, 2796 (2011).
[12] Q. Mei, C. J. Benmore, J. K. R. Weber, M. Wilding, J. Kim, and J. Rix, J. Phys.: Condens. Matter **20**, 245107 (2008).
[13] J. W. E. Drewitt, S. Jahn, V. Cristiglio, A. Bytchkov, M. Leydier, S. Brassamin, H. E. Fischer, and L. Hennet, J. Phys.: Condens. Matter **23**, 155101 (2011).; **24**, 099501 (2012).
[14] H. E. Fischer, A. C. Barnes, and P. S. Salmon, Rep. Prog. Phys. **69**, 233 (2006).
[15] T. Voigtmann, A. Meyer, D. Holland-Moritz, S. Stüber, T. Hansen, and T. Unruh, Europhys. Lett. **82**, 66001 (2008).
[16] S. Gruner, J. Marczinke, L. Hennet, W. Hoyer, and G. J. Cuello, J. Phys.: Condens. Matter **21**, 385403 (2009).
[17] V. F. Sears, Neutron News **3**, 26 (1992).
[18] M. C. Eckersley, P. H. Gaskell, A. C. Barnes, and P. Chieux, Nature (London) **335**, 525 (1988).
[19] P. H. Gaskell, M. C. Eckersley, A. C. Barnes, and P. Chieux, Nature (London) **350**, 675 (1991).
[20] L. B. Skinner, C. J. Benmore, J. K. R. Weber, S. Tumber, L. Lazareva, J. Neuefeind, L. Santodonato, J. Du, and J. B. Parise, J. Phys. Chem. B **116**, 13439 (2012).
[21] T. E. Faber and J. M. Ziman, Philos. Mag. **11**, 153 (1965).
[22] D. R. Neuville, G. S. Henderson, L. Cormier, and D. Massiot, Am. Mineral. **95**, 1580 (2010).
[23] H. E. Fischer, G. J. Cuello, P. Palleau, D. Feltin, A. C. Barnes, Y. S. Badyal, and J. M. Simonson, Appl. Phys. A: Mater. Sci. Process. **74**, s160 (2002).
[24] L. Hennet, I. Pozdnyakova, A. Bytchkov, V. Cristiglio, P. Palleau *et al.*, Rev. Sci. Instrum. **77**, 053903 (2006).
[25] A. Zeidler, J. Appl. Crystallogr. **45**, 122 (2012).
[26] A. Zeidler, J. W. E. Drewitt, P. S. Salmon, A. C. Barnes, W. A. Crichton, S. Klotz, H. E. Fischer, C. J. Benmore, S. Ramos, and A. C. Hannon, J. Phys.: Condens. Matter **21**, 474217 (2009).
[27] S. Jahn and P. M. Madden, Phys. Earth Planet. Inter. **162**, 129 (2007).
[28] G. J. Martyna, D. J. Tobias, and M. L. Klein, J. Chem. Phys. **101**, 4177 (1994).
[29] P. Courtial and D. B. Dingwell, Geochim. Cosmochim. Acta **59**, 3685 (1995).
[30] P. Courtial and D. B. Dingwell, Am. Mineral. **84**, 465 (1999).
[31] M. G. Tucker, D. A. Keen, M. T. Dove, A. L. Goodwin, and Q. Hui, J. Phys.: Condens. Matter **19**, 335218 (2007).
[32] J. W. E. Drewitt, C. Sanloup, A. Bytchkov, S. Brassamin, and L. Hennet, Phys. Rev. B **87**, 224201 (2013).
[33] P. S. Salmon, Proc. R. Soc. London, Ser. A **445**, 351 (1994).
[34] Q. Mei, C. J. Benmore, J. Siewenie, J. K. R. Weber, and M. Wilding, J. Phys.: Condens. Matter **20**, 245106 (2008).
[35] A. C. Hannon and J. M. Parker, J. Non-Cryst. Solids **274**, 102 (2000).

[36] C. J. Benmore, J. K. R. Weber, S. Sampath, J. Siewenie, J. Urquidi, and J. A. Tangeman, J. Phys.: Condens. Matter **15**, S2413 (2003).
[37] E. Lorch, J. Phys. C: Solid State Phys. **2**, 229 (1969).
[38] P. Kidkhunthod, L. B. Skinner, A. C. Barnes, W. Klysubun, and H. E. Fischer, Phys. Rev. B **90**, 094206 (2014).
[39] D. R. Neuville, L. Cormier, D. De Ligny, J. Roux, A.-M. Flank, and P. Lagarde, Am. Mineral. **93**, 228 (2008).
[40] L. B. Skinner, A. C. Barnes, P. S. Salmon, H. E. Fischer, J. W. E. Drewitt, and V. Honkimäki, Phys. Rev. B **85**, 064201 (2012).
[41] J. F. Stebbins, Chem. Geol. (2016), doi:10.1016/j.chemgeo.2016.06.029.
[42] J. C. Mauro, Am. Ceram. Soc. Bull. **90**, 31 (2011).
[43] J. C. Phillips and M. F. Thorpe, Solid State Commun. **53**, 699 (1985).
[44] L. Hennet, J. W. E. Drewitt, D. R. Neuville, V. Cristiglio, J. Kozaily, S. Brassamin, D. Zanghi, and H. E. Fischer, J. Non-Cryst. Solids **451**, 89 (2016).
[45] J. W. E. Drewitt, S. Jahn, C. Sanloup, C. de Grouchy, G. Garbarino, and L. Hennet, J. Phys.: Condens. Matter **27**, 105103 (2015).
[46] J. W. E. Drewitt, A. C. Barnes, V. Cristiglio, H. E. Fischer, L. Hennet, S. C. Kohn, and D. Neuville, Neutron diffraction with isotope substitution study of levitated liquid $CaAl_2O_6$, (2015), doi:10.5291/ILL-DATA.6-05-956.